Magnesium isotopic composition of oceanic mantle and oceanic Mg cycling

Ping-Ping Liu[a,b,c*], Fang-Zhen Teng[d*], Henry J. B. Dick[e], Mei-Fu Zhou[f], Sun-Lin Chung[c]

[a] *Key Laboratory of Orogenic Belts and Crustal Evolution, Peking University, Beijing 100871, China*

[b] *State Key Laboratory of Lithospheric Evolution, Institute of Geology and Geophysics, Chinese Academy of Sciences, Beijing 100029, China*

[c] *Institute of Earth Sciences, Academia Sinica, Taipei, Taiwan*

[d] *Isotope Laboratory, Department of Earth and Space Sciences, University of Washington, Seattle, WA, 98195, USA*

[e] *Department of Geology and Geophysics, Woods Hole Oceanographic Institution, Woods Hole, Massachusetts 02543, USA*

[f] *Department of Earth Sciences, the University of Hong Kong, Pokfulam Road, Hong Kong*

(5669 words for the main text)

*Corresponding author:

Ping-Ping Liu

Current address: Institute of Earth Sciences, Academia Sinica, 128, Sec. 2, Academia Road, Nangang, Taipei 11529, Taiwan

Email: liupingping11@live.cn

Fang-Zhen Teng

Address: Isotope Laboratory, Department of Earth and Space Sciences, University of Washington, Seattle, WA98195, USA

Email: fteng@u.washington.edu

Abstract

To constrain the Mg isotopic composition of the oceanic mantle, investigate Mg isotope fractionation of abyssal peridotites during seafloor alteration, and assess Mg budget in the oceans, a suite of 32 abyssal peridotite samples from the Gakkel Ridge and Southwest Indian Ridge (SWIR) was, for the first time, selected for high-precision Mg isotope analyses. Although most of these samples are extensively altered, largely by serpentinization and weathering, primary olivine, diopside and enstatite grains are preserved in some samples. Olivine grains from the least altered samples have δ^{26}Mg varying from -0.30 to -0.12 ‰ (*n*=7), whereas enstatite and diopside have δ^{26}Mg varying from -0.27 to -0.16 ‰ (*n*=7), and from -0.23 to -0.09 ‰ (*n*=6), respectively. Whole-rock δ^{26}Mg values range from -0.24 to 0.03 ‰ with an average of -0.12 ± 0.13 ‰ (2SD, *n*=32). Strongly serpentinized peridotites have lower average δ^{26}Mg values (δ^{26}Mg = -0.19 ± 0.07 ‰, 2SD, *n*=7) than weathering-dominated ones (δ^{26}Mg = -0.10 ± 0.12 ‰, 2SD, *n*=25). Calculated Mg isotopic compositions of fresh mantle peridotites vary from -0.29 to -0.13 ‰, beyond the previously reported range of the subcontinental lithospheric mantle (-0.25 ± 0.04 ‰) and the analytical uncertainty (± 0.07 ‰, 2SD). Our study therefore indicates that the oceanic mantle may have similar but slightly heterogeneous Mg isotopic compositions to that of subcontinental lithospheric mantle. Secondary serpentinization does not fractionate Mg isotopes of abyssal peridotites, whereas low-T weathering and formation of clay can result in the enrichment of heavy Mg isotopes in abyssal peridotites. This study also demonstrates that fluid-rock interaction does not

necessarily produce rocks with intermediate Mg isotopic compositions. Magnesium isotopes of the rocks thereafter are dependent on the secondary minerals formed. We also conclude that the release of light Mg isotopes into the ocean during alteration of abyssal peridotites can be an important influx of Mg for the seawater Mg budget. Abyssal peridotites with a heavy Mg isotopic signature can be recycled into the mantle in subduction zones and may thus result in heterogeneous Mg isotopic compositions of the oceanic mantle and heavy Mg isotopic compositions of arc magmas.

Keywords: abyssal peridotite, magnesium isotope, mantle heterogeneity, magnesium cycling, seafloor alteration

1. Introduction

Abyssal peridotites comprise an important part of the oceanic crust and thus have experienced prolonged fluid-rock interactions before being recycled as one of the components into subduction zones (e.g., Snow and Dick, 1995; Mével, 2003; Bach et al., 2004; Li and Lee, 2006; Paulick et al., 2006). The fluid-peridotite interaction has important consequences on the chemical budgets of oceans (Thompson and Melson, 1970; Snow and Dick, 1995), and is believed to be dominated by hydration reactions of olivine and pyroxenes that lead to formation of serpentine at a relatively broad range of temperatures (25 to 400 ℃, Klein et al., 2009), or weathering, represented by the formation of clay minerals at relatively low temperatures (e.g., Snow and Dick,

1995). Because abyssal peridotites are largely serpentinized and/or weathered oceanic mantle rocks, their compositions are considered as complex records of the overprinting processes of partial melting, melt-rock reaction, and melt refertilization in the asthenosphere and lithosphere, followed by hydrothermal alteration and weathering as they are uplifted and exposed on the seafloor (e.g., Hellebrand et al., 2001; Craddock et al., 2013). Therefore, abyssal peridotites provide a window for probing high-T mantle processes in relation with low-T hydrothermal alteration.

Magnesium is the most abundant element besides Si in abyssal peridotites. Previous studies have indicated that serpentinization is not an isochemical process with mass transfer of Ca, Na, Fe and Mn and decrease of MgO/SiO_2 ratio (Malvoisin, 2015). Marine weathering, on the other hand, is widely accepted to result in Mg loss (Snow and Dick, 1995). Previous isotopic studies have shown that the Earth's subcontinental lithospheric mantle has δ^{26}Mg values of -0.25 ± 0.04 ‰ (Teng et al., 2010a). However, oceanic peridotites of Purang (Tibet) have slightly higher δ^{26}Mg values of -0.20 ± 0.10 ‰ (Su et al., 2015), and altered oceanic crust has mantle-like Mg isotopic compositions with δ^{26}Mg ranging much wider from -2.76 to +0.21 ‰ (Huang et al., 2015; Teng, 2017). Magnesium isotopic composition of oceanic mantle peridotites and the behavior of Mg isotopes during fluid-peridotite interactions in the exposure of abyssal peridotites is poorly known so far. Studies of Mg isotopes of terrestrial ultramafic rocks indicate that Mg isotope fractionation strongly depends on the processes the rocks have undergone. Serpentinization was suggested not to fractionate Mg isotopes whereas carbonation can result in isotopically heavy talc and

isotopically light magnesite (Beinlich et al., 2014). In addition, metasomatism of mantle rocks is widely used to explain rocks with significant inter-mineral fractionation to light Mg isotopic compositions (Xiao et al., 2013; Beinlich et al., 2014; Wang et al., 2014; Hu et al., 2016a), whereas the influence of seawater on Mg isotopes of oceanic basalts and abyssal peridotites so far was suggested to be very limited due to the low Mg concentrations of seawater ([Mg] = 53 mmol/l or MgO = 0.21 wt.%) (Huang et al., 2015). However, a preliminary study by Wimpenny et al. (2012) indicated that weathering of abyssal peridotites is comparable to weathering of continental crust. This controversy mainly results from the limited database for Mg isotopic compositions of abyssal peridotites.

To understand the Mg isotopic systematics of the abyssal peridotites and its fractionation during seawater-rock interactions, we selected samples from four sites of the Gakkel Ridge and SWIR for whole-rock and mineral Mg isotopic analyses, and then calculated Mg isotopes of fresh oceanic mantle peridotites according to the mineral percentage and Mg isotopes of the constituting minerals. Our studies show that oceanic mantle may have slightly heterogeneous Mg isotopes and that significant amount of light Mg isotopes has been released to the ocean through seawater-peridotite interactions during the exposure of abyssal peridotites.

2. Geological background

The peridotites used in this study come from the Prince Edward (46.54°S, 33.79°E) and the Shaka Fracture Zones (FZs) (53.38°S, 9.33°E) on the

118 ultraslow-spreading Southwest Indian Ridge (SWIR), and three areas (84.64 ℃N,
119 4.22 ℃E, 84.83 ℃N, 4.66 ℃E and 85.44 ℃N, 14.52E) in the Sparsely Magmatic Zone of the
120 ultraslow-spreading Gakkel Ridge (Fig. 1). Detailed studies of these abyssal
121 peridotites and their respective locations have been presented in previous publications
122 (e.g., Hellebrand et al., 2001; Thiede et al., 2002; Dick et al., 2003; Michael et al.,
123 2003; Liu et al., 2008).

124 The SWIR separates the African and Antarctic plates, and spreads at a full rate of
125 14 mm yr^{-1}, making it an ultraslow spreading ridge (Dick et al., 2003). Sixteen abyssal
126 peridotites in this study are from two areas of the SWIR collected on cruise 107 Leg 5
127 of the RV Atlantis II (AII107), and Protea Expedition, Leg 5 (Pr) of the RV Melville
128 from the Shaka and Prince Edward FZs, respectively (Dick et al., 1984). Peridotites of
129 the SWIR range from lherzolites to harzburgites and exhibit major element
130 heterogeneity in the initial mantle, preserved because of low degrees of melting
131 beneath the SWIR (Seyler et al., 2003). The Gakkel Ridge in the high Arctic Ocean
132 extends east for ~1800 km from the Lena trough, north of Greenland, toward the
133 continental margin of the Laptev Sea (Thiede et al., 2002). Full spreading rate
134 decreases west to east from 14.6 to 6.3 mm yr^{-1}, making the entire ridge ultra-slow
135 spreading (Dick et al., 2003). There are three distinct regimes with different relative
136 abundances of rock types: a western volcanic zone, a central sparsely magmatic zone
137 that is nearly amagmatic and an eastern zone of widely spaced volcanoes (Michael et
138 al., 2003). Fourteen abyssal peridotites from the Gakkel Ridge in this study are from
139 the central sparsely magmatic zone collected during the AMORE Expedition of the

USCGC Healy (HLY) and RV Polarstern (PS) (Thiede et al., 2002; Michael et al., 2003). These peridotites include both depleted harzburgites and more fertile lherzolites, and are inferred to have undergone low-degree melting in the current ridge event due to the missing or overall thin crust along the ridge (Dick et al., 2003; Michael et al., 2003). The Gakkel Ridge peridotites come from amagmatic to weakly magmatic spreading segments, while the samples from SWIR are from large off-set transforms that likely inhibited mantle melting due to the transform edge effect (e.g., Dick et al., 2010). The two suites from the SWIR, on the other hand, represent low degree melting adjacent to the Shaka FZ, and moderately high degree melting adjacent to the Prince Edward FZ. Given their overall range in composition from diopside-poor harzburgite to diopside-rich lherzolite and the relatively thin crust at both ridges, it is likely that their mantle sources had undergone previous melting events prior to mantle melting during the current ridge event (e.g., Zhou and Dick, 2013).

Radiogenic isotopic studies (Sr, Nd, Pb and Os isotopes) of abyssal peridotites have demonstrated their heterogeneity in both large and small scales, with similar ranges to MORBs but extend to more depleted composition (e.g., Meyzen et al., 2005; Liu et al., 2008; Warren et al., 2009). Iron stable isotopes of abyssal peridotites (δ^{56}Fe = 0.010 ± 0.007 ‰) are indistinguishable from chondrites (Craddock et al., 2013). Debret et al. (2016) also indicated that ocean-floor serpentinization, represented by the formation of lizardite, does not fractionate Fe isotope appreciably. On the contrary, O and Li stable isotopes display signatures of interaction of abyssal peridotites with

serpentinizing fluids, leading to low $\delta^{18}O$ values (e.g. 3.7 to 2.6 ‰ for abyssal peridotites from the Mid-Atlantic Ridge) (Agrinier and Cannat, 1997) and low $\delta^{6}Li$ values (e.g. -2.9 to -14 ‰ for abyssal peridotites from SWIR) (Decitre et al., 2002).

3. Petrography

Most of the abyssal peridotites from the SWIR and Gakkel Ridge are 60 to 90% altered to clay and serpentine, while some are quite fresh, with only a few percent serpentine and light olivine weathering (e.g., PS59 235-4, Fig. 1). The majority of our samples are protogranular or porphyroclastic, together with some mylonites that have undergone intense ductile deformation The fresh samples contain coarse-granular enstatite and diopside that are typically 2-5 mm in size. Olivine in the fresh samples is well preserved with a microfracture network of black to brown alteration veins that crisscross the olivine. These veins are filled with serpentine, Fe-oxides and oxidized brown clay such as chlorite. Spinel occurs in minor amount and is mostly small and fresh.

In the altered abyssal peridotites, rock color often indicates the degree of serpentinization and/or weathering: orange to brown color indicates moderate to high weathering of silicate minerals to clay (e.g. AII107 from Shaka FZ, Fig. 1), while green and black colors indicate fresher, less weathered highly serpentinized rocks (e.g. Pr from Prince Edward FZ, Fig. 1). In the serpentinization-dominated samples, alteration minerals include serpentine, hornblende, andradite, chlorite and Cr-Fe oxides (Fig. 2a), whereas in weathering-dominated ones, alteration minerals are

184 similar but there are more chlorite and clusters of microcrystalline Mg-Si-Al-Cr-Fe
185 minerals that resemble iddingsite (Fig. 2b-d), a typical weathering product of
186 mafic-ultramafic rocks. About 62% of the Polar Stern peridotites are weathered to
187 different degrees and only 35% are serpentinized (Thiede et al., 2002), similar to the
188 Healy samples (Michael et al., 2003). The Gakkel Ridge and Shaka FZ peridotites in
189 this study are dominated by weathering, resulting in orangish-brown to tan coloring,
190 with subordinate serpentine alteration, while peridotites from the Prince Edward FZ
191 have primarily undergone serpentinization, consistent with their green to back colors
192 in hand samples.
193

194 ## 4. Analytical methods

195 Major element concentrations and loss-on-ignition (LOI) of the peridotites were
196 determined at Department of Geosciences, National Taiwan University, Taiwan.
197 Major element oxides were measured on fused glass disks using a Rigaku® RIX 2000
198 X-ray fluorescence (XRF) spectrometer. LOI was obtained by routine procedures.
199 Analytical uncertainties were estimated to be better than 5% (relative) for XRF
200 analyses (Lee et al., 1997).

201 All chemical procedures including sample dissolution, column chemistry and
202 instrumental analysis of Mg isotopes were conducted at the Isotope Laboratory of the
203 University of Washington, Seattle, following the procedures of previous studies (Teng
204 et al., 2007, 2010a, 2015). Weathered/alteration rinds and carbonate veins were cut off
205 prior to crushing. Mineral separates were cleaned three times (3×10min) in Milli-Q

206 water with an ultrasonic bath. Sample dissolution and column chemistry were carried
207 out in the clean lab. Mineral separates were cleaned in an ultrasonic bath to remove
208 alteration from grain boundaries and cracks. About 1 to 3 mg whole-rock powder or
209 mineral separates were dissolved in a mixture of Optima-grade concentrated
210 HF-HNO_3-HCl in sealed 7 ml Savillex Teflon$^{@}$ screw-top capsule on a 100 ℃ hot
211 plate in a laminar flow exhaust hood. After complete dissolution, the samples were
212 dried out and redissolved in 1 N HNO_3 before chromatographic separation. Chemical
213 separation of Mg was achieved by cation exchange chromatography using Bio-Rad
214 AG50W-X8 (200 to 400 mesh) resin in 1 N HNO_3. The same purification procedure
215 was performed twice to effectly remove matrix elements. The total procedural blank
216 was < 10 ng for Mg, representing <0.1% Mg loaded onto the columns. Detailed
217 processing methods can also be referred to Hu et al. (2016a) and references therein.
218 Magnesium isotopic compositions were analyzed using the sample-standard
219 bracketing method on a *Nu Plasma II* MC-ICPMS at the University of Washington
220 (Teng and Yang, 2014). Two standards, San Carlos olivine and Hawaiian seawater
221 which were processed together with the samples through column chemistry, were
222 analyzed with each batch of samples to monitor the accuracy and reproducibility. An
223 international standard of JB-1 basalt powder was also processed through the same
224 procedure with the rock samples to access the accuracy of Mg isotopic analyses.
225 Magnesium isotopic data are reported in delta (δ) notation in per mil relative to DSM3
226 standard (a solution in 3% HNO_3 made from pure Mg metal, Galy et al., 2003): $\delta^{26}Mg$
227 (‰) = $[(^{26}Mg/^{24}Mg)_{sample}/(^{26}Mg/^{24}Mg)_{DSM\text{-}3}\text{-}1] \times 1000$. Results for these standards are

in agreement with previously published data (Table 1). Repeated analyses indicate data reproducibility is better than ±0.07 ‰ (2 standard deviations, SD) for δ^{26}Mg (Teng et al., 2015).

5. Results

5.1 Whole-rock major element compositions

The peridotites in this study show large variations in SiO_2 (32.4 to 51.8 wt.%), MgO (25.7 to 46.5 wt.%), Fe_2O_3 (6.80 to 12.6 wt.%), Al_2O_3 (0.17 to 5.22 wt.%), TiO_2 (0 to 0.17 wt.%), and CaO (0.49 to 16 wt.%), with LOI varying from 0.9 to 18.2 wt.% (Appendix 1). Recalculated to volatile free compositions, the average compositions of SiO_2 (44.0 ± 2.8 1σ wt.%), MgO (39.6 ± 3.9 wt.%), Fe_2O_3 (10.3 ± 1.4 wt.%), Al_2O_3 (1.9 ± 1.1 wt.%), TiO_2 (0.07 ± 0.04 wt.%) and CaO (4.0 ± 4.5 wt.%) range much larger than for fresh or reconstructed abyssal peridotite compositions, which have quite restricted ranges for most major elements (Snow and Dick, 1995). In particular, our samples have on average lost Mg, gained Al and Ca.

5.2 Whole-rock Mg isotopic compositions

Magnesium isotopic compositions of reference samples and abyssal peridotites are reported in Table 1. δ^{26}Mg values of abyssal peridotites display wide variations from -0.24 to 0.03 ‰ with an average value of -0.12 ± 0.13 ‰ (2SD, *n* = 32) (Fig. 3). In particular, rocks from the Prince Edward FZ (Pr 18 and Pr 19) that undergone intense serpentinization with less weathering have, on average, lighter Mg isotopic compositions (δ^{26}Mg = -0.24 to -0.14 ‰ with an average of -0.19 ± 0.07 ‰, 2SD, *n* =

7) than abyssal peridotites from other localities (δ^{26}Mg = -0.21 to 0.03 ‰ with an average of -0.10 ± 0.12 ‰, 2SD, *n* = 25). These values are slightly heavier than average values of oceanic basalts and mantle peridotites (δ^{26}Mg = -0.25 ± 0.07‰) reported in previous studies (e.g., Handler et al., 2009; Yang et al., 2009; Teng et al., 2010a; Huang et al., 2011; Lai et al., 2015)

5.3 Mineral magnesium isotopic composition

Magnesium isotopic compositions of olivine, enstatite and diopside from seven relatively fresh abyssal peridotites vary in a small but discernible range. Olivine and enstatite have δ^{26}Mg values from -0.30 to -0.12 ‰ and -0.27 to -0.16 ‰, respectively, slightly lower than that of diopside (δ^{26}Mg = -0.23 to -0.09 ‰) (Table 2). Although slight variation exists for the same mineral from different samples, the δ^{26}Mg values of olivine and enstatite are similar and within the mantle Mg isotopic range, slightly lower than that of diopside, consistent with existing published data (Handler et al., 2009; Yang et al., 2009; Huang et al., 2011; Liu et al., 2011; Xiao et al., 2013; Hu et al., 2016b) and equilibrium theoretical predictions (Schauble, 2011; Huang et al., 2013). Whole-rock Mg isotopic compositions for the primary mantle peridotites are calculated according to mineral percentage and δ^{26}Mg values of the constituting minerals in order to eliminate the effect of late-stage alteration along the cracks of olivine. The calculation results show that mantle peridotites have slightly varied whole-rock δ^{26}Mg values from -0.29 to -0.13 ‰ (Table 2), beyond the analytical uncertainty (± 0.07 ‰) acquired in our lab.

6. Discussion

The heavy Mg isotopic composition of abyssal peridotites compared to Earth's mantle (δ^{26}Mg = -0.25 ± 0.04 ‰, Teng et al., 2010a) is unexpected, considering its reaction with isotopically light seawater (δ^{26}Mg = -0.83 ± 0.09 ‰, Ling et al., 2011). The diversity of samples with variable degrees of alteration allow us to discuss the Mg isotopic composition of the oceanic mantle, the behavior of Mg isotopes during seawater alteration, the implications of Mg isotope fractionation during seawater-peridotite interaction for other fluid-rock interaction processes, and finally the impact of this study on Mg isotopic recycling in the mantle and oceans.

6.1 Whole-rock major element composition

The large range in silicon and calcium content, recalculated to 100% volatile free, indicates that both these elements are mobile during alteration. None of the minerals in a generic peridotite have less than 40 wt.% SiO_2, and the proportion of pyroxene to olivine in abyssal peridotites is such that the SiO_2 content of fresh peridotite is generally between 43 and 44 wt.%, while CaO is generally less than 3 wt.%. In our samples, silica ranges from 32 to 52 wt.% and CaO from near zero to almost 20 wt.% (Fig. 4a,b). Calcium versus silica also produces no significant correlation (Fig. 4a). Aluminium has not remained constant, increasing to values much higher than seen in any reconstructed abyssal peridotite composition, with up to 5.33 wt.% Al_2O_3 in sample PS59 235-4. The average aluminium for the suite is at the top of the observed range for reconstructed fertile lherzolite compositions.

294 From this, it is clear that alteration of our samples was not isochemical, and that
295 silica should not be assumed constant during serpentinization. Both aluminium and
296 titanium, however, are relatively immobile elements, and tend to be redistributed
297 among the mineral phases during alteration, rather than being lost or gained. This is
298 illustrated in Figure 4c, where there is a good correlation between these elements.
299 Calcium and aluminium, with the exception of four outliers from the Gakkel Ridge
300 which were considered to have undergone carbonate alteration, also display a good
301 positive correlation (Fig. 4b). These correlations are consistent with residues of partial
302 melting, and the large range in degrees of melting inferred for these and other abyssal
303 peridotites from mineral modes and compositions (e.g., Dick et al., 1984). Based on
304 these correlations, the increase in aluminium in the altered peridotites likely reflects
305 its immobility rather than any actual addition, during alteration, hydration, and loss of
306 other species.

307 Four of the Protea Leg 5 samples have elevated TiO_2 and higher alumina than the
308 remaining three (Fig. 4c), all of which have relatively light δ^{26}Mg (Fig. 4d). The high
309 titanium can be explained in a number of ways, but one likely source is impregnation
310 by a MORB-like melt, which also means that plagioclase was present in the unaltered
311 peridotite (Dick, 1989). Generally, fresh plagioclase is not present in abyssal
312 peridotites, as it readily alters to prehnite and/or hydrogrossular ± chlorite and clay.
313 Hence, this reaction could affect the Mg isotopic composition of the altered rock, and
314 could be a possible source of lighter isotopic compositions in some abyssal peridotites.
315 Otherwise, no consistent correlation can be seen between relatively immobile major

316 elements and the isotopic composition of our samples, consistent with there being no
317 relationship to igneous petrogenesis (e.g., Fig. 4d).
318
319 **6.2 Mantle Mg isotopic heterogeneity**
320 Previous studies on Mg isotopic composition of the Earth's mantle have analyzed
321 mineral separates and whole-rock compositions of mantle xenoliths from
322 subcontinental lithospheric mantle as representative of the Mg isotopic composition of
323 the upper mantle, or comparison to chondrites (Handler et al., 2009; Yang et al., 2009;
324 Teng et al., 2010a; Huang et al., 2011; Liu et al., 2011; Xiao et al., 2013; Hu et al.,
325 2016a). This indirect sampling is largely because of the inaccessibility of mantle rocks.
326 Although mantle xenoliths entrapped in lavas commonly display varied Mg isotopic
327 compositions due to metasomatism and/or contamination during their ascent to the
328 Earth's surface, particularly near subduction zones where intense fluid activities occur
329 (e.g., Yaxley et al., 1991; Ionov et al., 1993; Rudnick et al., 1993), relatively
330 homogeneous Mg isotopic compositions of -0.25 ± 0.04 ‰ for global peridotite
331 xenoliths from subcontinental lithospheric mantle have been reported by Teng et al.
332 (2010a). Fresh minerals of abyssal peridotites from oceanic mantle, however, are not
333 influenced by these processes. In addition, the fresh mineral separates are not affected
334 by serpentinization or weathering, and thus can provide Mg isotopic compositions of
335 the primary oceanic mantle. The seven relatively fresh abyssal peridotites from SWIR
336 and Gakkel Ridge in this study have homogeneous olivine, enstatite, diopside and
337 spinel compositions in each sample and within the range of typical mantle rocks

(Appendix 2). Mineral compositions of the coexisting silicates indicate they are fresh, in equilibrium and have not been modified by late-stage processes. Orthopyroxene-olivine and clinopyroxene-olivine Mg isotopic fractionations largely fall along the theoretically calculated fractionation line by Schauble (2011) (Fig. 5a, b), indicating equilibrium Mg isotopic fractionation between the coexisting silicate minerals for these mantle peridotites. Mantle olivine, however, has Mg isotopic compositions varying from -0.12 to -0.30 ‰, beyond the analytical uncertainty (± 0.07 ‰). Similarly, whole-rock Mg isotopes of these mantle peridotites calculated through mineral percentage and isotopic composition display heterogeneous variation (-0.29 to -0.13 ‰) that is beyond the subcontinental mantle range (δ^{26}Mg = -0.25 ± 0.04 ‰, Teng et al., 2010a) and is not related to partial melting degrees represented by Cr# of spinel (Fig. 5c). If Mg isotopes do not fractionate during partial melting and melt extraction of the mantle rocks as previously demonstrated (Handler et al., 2009; Yang et al., 2009; Xiao et al., 2013; Lai et al., 2015) and this study shows, the Mg isotopic signature of the olivine crystals and whole-rock mantle peridotites under the Gakkel Ridge and the SWIR may represent heterogeneous oceanic mantle. This Mg isotopic heterogeneity may result from the subduction and residence of oceanic lithosphere in the mantle, which brings abundant MgO in isotopically heavy abyssal peridotite and altered basalt and less MgO in isotopically light/heavy marine sediments back into the convecting mantle. Similar phenomenon of O, Li and Fe stable isotopic heterogeneity has already been reported in mantle rocks (Krienitz et al., 2012; Williams and Bizimis, 2014). Because of the large amount of Mg in abyssal

360 peridotites and altered basalts and the high density, their recycling into the mantle
361 may shift the Mg isotopes of mantle source to a heavier value and provide sources of
362 heavy Mg isotopes for arc magmas. This has just been identified by Teng et al. (2016)
363 in Lesser Antilles Arc lava, which displays a wide range of δ^{26}Mg (-0.25 to -0.10 ‰)
364 slightly heavier than the mantle value.
365
366 **6.3 Magnesium loss and Mg isotopic fractionation of abyssal peridotites**
367 **during seawater alteration**
368 Abyssal peridotites recovered from different localities of the mid-ocean ridges
369 represent exposed mantle rocks that have variably experienced post-magmatic
370 hydrothermal alteration (e.g., Snow and Dick, 1995; Humphris and Bach, 2004).
371 Because of a relatively restricted δ^{26}Mg range of mantle source, any Mg isotopic
372 variation, if present, should reflect subsequent alteration process en route to and/or
373 exposed on the seafloor. The average δ^{26}Mg value of 32 abyssal peridotites is -0.12 ±
374 0.13 ‰ (2SD, n = 32) and the Mg isotopic fractionation can be resolvable by up to
375 0.27 ‰, far beyond the analytical precision acquired (±0.07 ‰). Paulick et al. (2006)
376 have summarized that an initial stage of high-temperature (> 375 - 400 ℃)
377 hydrothermal interaction of peridotite with hydrothermal solutions results in
378 widespread serpentinization; the last stage of alteration is low-T (< 150 ℃) interaction
379 of the serpentinites with ambient seawater that circulates in the near seafloor
380 environment, generating aragonite veinlets, Fe-oxyhydroxides and clays. Therefore,
381 serpentinization and seafloor weathering are evaluated separately to interpret Mg

isotope fractionation of abyssal peridotites.

6.3.1 Serpentinization

Serpentinites are abundantly exposed at slow and ultraslow spreading ridges, largely produced by hydrothermal circulation into mantle rocks during faulting and uplift to the seafloor and alteration of oceanic lithosphere (e.g., Dick et al., 2003; Zhou and Dick, 2013; Debret et al., 2016). The fluid responsible for serpentinization is seawater, possibly evolved by interaction with the crust. The extent of serpentinization in the abyssal peridotites is commonly assessed from LOI values (e.g., Craddock et al., 2013). It is noteworthy that for a given LOI value, the MgO contents vary in a large range of ~5 wt.% relative (Fig. 3a). Since marine weathering leading to the formation of clay (hydrous aluminium phyllosilicates) can also introduce water into the peridotites, the LOI value of abyssal peridotites cannot be simply considered as an index of serpentinization. Petrographic observations should be carried out to discriminate serpentinization and weathering before using simply geochemical parameters.

Serpentine minerals, dominated by lizardite, chrysotile and antigorite, consist of alternating infinite sheets of 4-coordinated Si and 6-coordinated Mg (Mével, 2003; Li et al., 2014). Among them, lizardite is a primary phase in seafloor serpentinites because it forms at low temperature and pressure (Mével, 2003). It has been well demonstrated that Mg isotopic fractionation is controlled by coordination and bonding environment (Liu et al., 2010, 2011; Li et al., 2011, 2016; Shauble, 2011; Huang et al.,

404 2013). Although the Mg isotopic composition of lizardite has not yet been reported, it
405 is speculated to be not significantly different from olivine, which also contains
406 6-coordinated Mg. This appears to be confirmed by our samples from Prince Edward
407 FZ (Pr in Fig. 3b), which have undergone intense serpentinization, have δ^{26}Mg values
408 within or minimally higher than the mantle range. Recent studies by Beinlich et al.
409 (2014) and Debret et al. (2016) also indicate that seafloor serpentinization does not
410 fractionate Mg and Fe isotopes, although increasing degrees of prograde
411 metamorphism resulting in the formation of antigorite may lead to loss of isotopically
412 light Fe to the fluids. Therefore, our study confirms that serpentinization is not likely
413 to fractionate Mg isotopes. We further propose that LOI cannot directly represent the
414 extent of serpentinization and that Mg isotopic fractionation in abyssal peridotites is
415 largely positively correlated with increasing volatile contents.
416
417 **6.3.2 Seafloor weathering**
418 Marine weathering of abyssal peridotites at the seafloor is known to affect
419 primary chemical compositions, leading to the loss of Mg from the rocks during this
420 process (Snow and Dick, 1995). Two types of low-temperature seafloor weathering
421 have been distinguished. One is dominated by weathering of olivine to iddingsite
422 (clay+goethite+aragonite), resulting in increase of Ca and loss of Si and Mg. The
423 other is characterized by weathering of serpentine and magnetite to talc + hematite ±
424 dolomite, with an increase in Si and Fe and a decrease in Mg (Humphris and Bach,
425 2004). The former has been identified petrographically as the primary weathering

426 process occurred in abyssal peridotites of this study (Figs. 1 and 2).

427 Seafloor weathering can be assessed by a plot of MgO/SiO_2 versus Al_2O_3/SiO_2 in
428 which weathering is characterized by departure from the terrestrial geochemical
429 fractionation array (Hart and Zindler, 1986). The proxy for weathering, MgO/SiO_2*,
430 is a quantitative measure of the departure of the measured peridotite MgO/SiO_2 ratio
431 from the primary ratio of each sample estimated from the MgO/SiO_2 versus
432 Al_2O_3/SiO_2 magmatic fractionation trend (Fig. 6a), assuming that Al and Si are
433 immobile during marine weathering (Snow and Dick, 1995). Our study shows that Mg
434 isotopes of variably weathered abyssal peridotites are slightly heavy with an average
435 $\delta^{26}Mg$ value of -0.12 ± 0.14 ‰ (2SD) compared with mantle peridotite value ($\delta^{26}Mg$
436 = -0.25 ± 0.04 ‰, Teng et al., 2010a). As MgO/SiO_2* ratios and the inferred degree of
437 weathering increase, the $\delta^{26}Mg$ ratios of abyssal peridotites increase as well (Fig. 6b).
438 This suggests that during seafloor weathering process, the Mg isotopic compositions
439 of the abyssal peridotites become heavy. Moreover, the negative correlation between
440 MgO content and $\delta^{26}Mg$ value indicates that heavy Mg isotope is enriched during
441 decrease of whole-rock MgO content (Fig. 6c). Therefore, the heavy Mg isotopic
442 compositions of abyssal peridotites could be due to the formation of iddingsite by
443 seafloor weathering. This is comparable to continental crust weathering, where clay
444 formation usually results in heavy Mg isotope enrichment compared with the mafic
445 protolith (e.g., Teng et al., 2010b; Huang et al., 2012; Liu et al., 2014).

446 The enrichment of heavy Mg isotope in residual clays and release of light Mg
447 isotope into the fluids during abyssal peridotite-fluids interactions can be modeled by

448 Rayleigh fractionation as it can for continental weathering. Using average MgO
449 concentration (44 wt.%, Snow and Dick, 1995) and δ^{26}Mg value in primary mantle
450 rocks, the apparent fractionation factor (α) obtained by modeling varies from ~1.0002
451 to 1.001 (Fig. 7), which corresponds to Mg isotopic fractionation between abyssal
452 peridotites and fluids from ~0.2 ‰ to 1 ‰. Accordingly, the fluids may contain Mg
453 isotopic compositions of -1.12 to -0.32 ‰. The large range in α value reflects a
454 complex process of dissolution of primary phases and precipitation of secondary
455 minerals and may therefore be a minimum (Liu et al., 2014).
456
457 **6.4 Implications for Mg isotopic fractionation during fluid-rock interactions**
458 The heavy Mg isotopic composition of abyssal peridotites relative to fresh
459 mantle peridotites indicates that during weathering of olivine, formation of clay
460 preferentially releases light Mg isotopes into seawater. This fractionation is mainly
461 driven by the difference in coordination environment between Mg in clay and
462 seawater. Mantle rocks with light Mg isotopes (lighter than mantle value) from
463 previous studies are usually explained as metasomatism by melts with light Mg
464 isotopic compositions (Xiao et al., 2013; Hu et al., 2016a). By contrast, mantle rocks
465 with heavy Mg isotopes are commonly interpreted as due to kinetic isotope
466 fractionation by diffusion during melt-peridotite interaction (Huang et al., 2011; Xiao
467 et al., 2013). Our study, however, indicates that rocks with heavier Mg isotopic
468 compositions do not need to react with melt/fluid that has high Mg content and heavy
469 Mg isotopic composition. Through reaction with isotopically light seawater, abyssal

peridotites can release light Mg isotopes into the ocean and retain heavy Mg isotopes in the weathering products of clay. This indicates that the Mg isotopic composition of a rock has no essential correlation with Mg content and Mg isotopic composition of the reacting melt/fluid, but is strongly dependent on the secondary minerals formed. Our study also indicates that rocks reacted with carbonate fluids with light Mg isotopic signature do not necessarily become enriched in light Mg isotopes, which is often explained as the reason for Mg-isotopically light mantle-derived rocks. Rather, other evidence for reaction with carbonate fluids needs to be provided together and the processes whether they were mixed or reacted and the secondary minerals formed after reaction also need to be investigated (e.g. Yang et al., 2012; Huang et al., 2015; Wang et al., 2016). If carbonate is formed as a secondary mineral resulting from carbonate metasomatism, the rock is expected to have light Mg isotopic composition, as has been shown by Xiao et al. (2013). Therefore, Mg isotopic composition of a rock or mineral should be interpreted together with detailed petrographical observation and identification of mineral assemblage.

6.5 Implications for oceanic Mg isotopic budget

Serpentinized peridotites are an important component of the oceanic crust at slow and ultraslow spreading ridges. Yet riverine Mg is considered to represent the main source for ocean's Mg budget (Tipper et al., 2006). Studies of Mg cycling in oceans used to focus on the discrepancy of riverine light Mg isotopic input (δ^{26}Mg = -1.09‰, Tipper et al., 2006) with global seawater of relatively heavier Mg isotopic

composition (δ^{26}Mg = -0.83 ‰, Ling et al., 2011). It is well recognized that precipitation of dolomite preferentially incorporates light Mg isotopes, thus maintaining the heavier Mg isotope budget of seawater compared to rivers (De Villiers et al., 2005; Tipper et al., 2006). In this study, we have shown that Mg isotopes of abyssal peridotites fractionate during seafloor weathering and light Mg isotope released by formation of isotopically heavy clays shifts the Mg isotope budget of the ocean to an opposite direction. If we assume the primary mantle peridotite has 44% MgO (Snow and Dick, 1995) with δ^{26}Mg = -0.25 ‰ and the abyssal peridotite contains 37% MgO with an average δ^{26}Mg = -0.12 ‰ (this study), the released Mg (5%) has an Mg isotopic ratio of -1.31 ‰. If the exposure of serpentinites could represent ~20% of the seafloor as suggested by Cannat et al. (1995) and similar weathering processes occurred on oceanic basalts and gabbros exposed on the seafloor, the Mg released during weathering could shift Mg isotopes of the ocean significantly to a lighter value. This indicates that deposition of light Mg isotopes from the ocean has been significantly underestimated. Therefore, studies on global Mg cycling and Mg isotopic budget of the oceans, in particular, need to take into account the release of light Mg isotope into the ocean during seafloor weathering of abyssal peridotites.

7. Conclusions

Our study has, for the first time, reported high-precision Mg isotopic compositions of abyssal peridotites from the Gakkel Ridge and SWIR. The main conclusions to be drawn include:

1) Abyssal peridotites display variable δ^{26}Mg values ranging from -0.24 to 0.03 ‰, with an average of -0.12 ± 0.13 ‰ (2SD, *n* = 32), heavier than those of subcontinental lithospheric mantle peridotites (δ^{26}Mg = -0.25 ± 0.04 ‰) reported by Teng et al. (2010a). The heterogeneous and heavier Mg isotopic compositions reflect Mg isotope fractionation during seafloor weathering, in which light Mg isotope was preferentially released to the ocean whereas heavy Mg isotope was retained in clay minerals, comparable to that of continental weathering on terrestrial planet.

2) The lack of Mg isotope fractionation in serpentinized abyssal peridotites suggests that alteration by serpentinization probably does not fractionate Mg isotopes, consistent with the study by Beinlich et al. (2014).

3) Fresh olivine grains and reconstructed fresh oceanic mantle peridotites have δ^{26}Mg values from -0.30 to -0.12 ‰ and -0.29 to -0.13 ‰, respectively, beyond the analytical uncertainty acquired (± 0.07 ‰) in our lab, indicating heterogeneous Mg isotopic compositions of the oceanic mantle source.

4) Mg isotope fractionation during melt/fluid-rock interaction is largely dependent on the secondary minerals formed, instead of δ^{26}Mg value of the interacting melt/fluid. Therefore, detailed petrographical observation and identification of mineral assemblage should be carried out before interpretation of Mg isotopic signature.

5) Release of light Mg isotope into the seawater during weathering of abyssal peridotite is an important influx of Mg to the ocean and influences its Mg content and Mg isotopic budget, which may need to be compensated by simultaneous deposition.

Further studies should take this into account when constructing Mg isotopic budget and evaluating Mg cycling of the oceans.

Acknowledgements

We are grateful to Drs. Kang-Jun Huang, Xiaochun Li, Shui-Jiong Wang and Hui Huang, Yang Sun. Mr. Aaron Brewer and Miss Yan Hu for their help in the clean lab and also for their helpful discussions during preparation of this manuscript. We thank Mr. Ben Urann from WHOI for helping with collecting the samples. Very detailed and constructive comments from three anonymous reviewers and efficient handling from associate editor Shichun Huang are greatly appreciated. This study was supported by grants from the National Science Foundation of China (grants 41473038 and 41503010), China Postdoctoral Science Foundation (2015M570145), National Science Foundation (EAR-1056713 and EAR-1340160) and project MOST104 -2745-M-002-001-ASP granted to SLC. Partial support for HJBD was provided by the US National Science Foundation (OCE-1434452).

References

Agrinier, P., Cannat, M., 1997. Oxygen-isotope constraints on serpentinization processes in ultramafic rocks from the Mid-Atlantic Ridge (23 N). Proc. Ocean Drill Prog Sci Results 153, 381-388.

Agrinier, P., Hékinian, R., Bideau, D., Javoy, M., 1995. O and H stable isotope compositions of oceanic crust and upper mantle rocks exposed in the Hess Deep near the Galapagos Triple Junction. Earth Planet. Sci. Lett. 136, 183-196.

Bach, W., Garrido, C.J., Paulick, H., Harvey, J., Rosner, M., 2004. Seawater-peridotite interactions: First insights from ODP Leg 209, MAR 15 N. Geochem. Geophy. Geosy. 5.

Beinlich, A., Mavromatis, V., Austrheim, H., Oelkers, E.H., 2014. Inter-mineral Mg isotope fractionation during hydrothermal ultramafic rock alteration–Implications for the global Mg-cycle. Earth Planet. Sci. Lett. 392, 166-176.

Cannat, M., Mevel, C., Maia, M., Deplus, C., Durand, C., Gente, P., Agrinier, P., Belarouchi, A., Dubuisson, G., Humler, E., 1995. Thin crust, ultramafic exposures, and rugged faulting patterns at the Mid-Atlantic Ridge (22–24 N).

569 Geology 23, 49-52.
570 Craddock, P.R., Warren, J.M., Dauphas, N., 2013. Abyssal peridotites reveal the
571 near-chondritic Fe isotopic composition of the Earth. Earth Planet. Sci. Lett. 365,
572 63-76.
573 De Villiers, S., Dickson, J., Ellam, R., 2005. The composition of the continental river
574 weathering flux deduced from seawater Mg isotopes. Chem. Geol. 216, 133-142.
575 Dick, H.J.B., 1989. Abyssal peridotites, very slow spreading ridges and ocean ridge
576 magmatism. in: Saunders, A.D., Norry, M.J. (Eds.), Magmatism in the Ocean
577 Basins, Geol. Soc. Spec. Publ. No. 42, 71-105.
578 Debret, B., Millet, M.-A., Pons, M.-L., Bouilhol, P., Inglis, E., Williams, H., 2016.
579 Isotopic evidence for iron mobility during subduction. Geology 44, 215-218.
580 Decitre, S., Deloule, E., Reisberg, L., James, R., Agrinier, P., Mével, C., 2002.
581 Behavior of Li and its isotopes during serpentinization of oceanic peridotites.
582 Geochem. Geophy. Geosy. 3, 1-20.
583 Dick, H.J.B., Fisher, R.L., Bryan, W.B., 1984. Mineralogic variability of the
584 uppermost mantle along mid-ocean ridges. Earth Planet. Sci. Lett. 69, 88-106.
585 Dick, H.J.B,, Lin, J., Schouten, H., 2003. An ultraslow-spreading class of ocean ridge.
586 Nature 426, 405-412.
587 Dick, H.J.B., Lissenberg, C.J., Warren, J., 2010. Mantle melting, melt transport and
588 delivery beneath a slow-spreading ridge: The Paleo-MAR from 23°15'N to
589 23°45'N. J. Petrol. 51, 425-467.
590 Galy, A., Yoffe, O., Janney, P.E., Williams, R.W., Cloquet, C., Alard, O., Halicz, L.,
591 Wadhwa, M., Hutcheon, I.D., Ramon, E., Carignan, J., 2003. Magnesium isotope
592 heterogeneity of the isotopic standard SRM980 and new reference materials for
593 magnesium-isotope-ratio measurements. J. Anal. At. Spectrom. 18, 1352-1356.
594 Handler, M.R., Baker, J.A., Schiller, M., Bennett, V.C., Yaxley, G.M., 2009.
595 Magnesium stable isotope composition of Earth's upper mantle. Earth Planet. Sci.
596 Lett. 282, 306-313.
597 Hart, S.R., Zindler, A., 1986. In search of a bulk-Earth composition. Chem. Geol. 57,
598 247-267.
599 Hellebrand, E., Snow, J.E., Dick, H.J., Hofmann, A.W., 2001. Coupled major and
600 trace elements as indicators of the extent of melting in mid-ocean-ridge
601 peridotites. Nature 410, 677-681.
602 Hu, Y., Harrington, M.D., Sun, Y., Yang, Z., Konter, J., Teng, F.Z., 2016b. Magnesium
603 isotopic homogeneity of San Carlos olivine: a potential standard for Mg isotopic
604 analysis by multi‐collector inductively coupled plasma mass spectrometry.
605 Rapid Commun. Mass Spectrom. 30, 2123-2132.
606 Hu, Y., Teng, F.-Z., Zhang, H.-F., Xiao, Y., Su, B.-X., 2016a. Metasomatism-induced
607 mantle magnesium isotopic heterogeneity: Evidence from pyroxenites. Geochim.
608 Cosmochim. Acta 185, 88-111.
609 Huang, F., Chen, L., Wu, Z., Wang, W., 2013. First-principles calculations of
610 equilibrium Mg isotope fractionations between garnet, clinopyroxene,
611 orthopyroxene, and olivine: Implications for Mg isotope thermometry. Earth
612 Planet. Sci. Lett. 367, 61-70.

Huang, F., Zhang, Z., Lundstrom, C.C., Zhi, X., 2011. Iron and magnesium isotopic compositions of peridotite xenoliths from Eastern China. Geochim. Cosmochim. Acta 75, 3318-3334.

Huang, J., Ke, S., Gao, Y., Xiao, Y., Li, S., 2015. Magnesium isotopic compositions of altered oceanic basalts and gabbros from IODP site 1256 at the East Pacific Rise. Lithos 231, 53-61.

Huang, K.-J., Teng, F.-Z., Wei, G.-J., Ma, J.-L., Bao, Z.-Y., 2012. Adsorption-and desorption-controlled magnesium isotope fractionation during extreme weathering of basalt in Hainan Island, China. Earth Planet. Sci. Lett. 359, 73-83.

Humphris, S., Bach, W., 2004. The geochemical consequences of serpentinization and weathering of oceanic peridotites, AGU Fall Meeting Abstracts, p. 0630.

Ionov, D.A., Dupuy, C., O'Reilly, S.Y., Kopylova, M.G., Genshaft, Y.S., 1993. Carbonated peridotite xenoliths from Spitsbergen: implications for trace element signature of mantle carbonate metasomatism. Earth Planet. Sci. Lett. 119, 283-297.

Klein, F., Bach, W., Jöns, N., McCollom, T., Moskowitz, B., Berquó, T., 2009. Iron partitioning and hydrogen generation during serpentinization of abyssal peridotites from 15°N on the Mid-Atlantic Ridge. Geochim. Cosmochim. Acta 73, 6868-6893.

Krienitz, M.-S., Garbe-Schönberg, C.-D., Romer, R., Meixner, A., Haase, K., Stroncik, N., 2012. Lithium isotope variations in ocean island basalts-implications for the development of mantle heterogeneity. J. Petrol. egs052.

Lai, Y.-J., von Strandmann, P.A.P., Dohmen, R., Takazawa, E., Elliott, T., 2015. The influence of melt infiltration on the Li and Mg isotopic composition of the Horoman Peridotite Massif. Geochim. Cosmochim. Acta 164, 318-332.

Lee, C.Y., Tsai, J.H., Ho, H.H., Yang, T.F., Chung, S.L., Chen, C.H., 1997. Quantitative analysis in rock samples by an X-ray fluorescence spectrometer (I) major elements, Program with Abstracts, Annual Meeting of Geological Society of China, Taipei, pp. 418-420.

Li, W.-Y., Teng, F.-Z., Xiao, Y., Huang, J., 2011. High-temperature inter-mineral magnesium isotope fractionation in eclogite from the Dabie orogen, China. Earth Planet. Sci. Lett. 304, 224-230.

Li, W.-Y., Beard, B.L., Li, C., Johnson, C.M., 2014. Magnesium isotope fractionation between brucite [$Mg(OH)_2$] and Mg aqueous species: Implications for silicate weathering and biogeochemical processes. Earth Planet. Sci. Lett. 394, 82-93.

Li, W.-Y., Teng, F.-Z., Xiao, Y., Gu, H.-O., Zha, X.-P., Huang, J., 2016. Empirical calibration of the clinopyroxene–garnet magnesium isotope geothermometer and implications. Contrib. Mineral. Petrol. 171, 61.

Li, Z.-X.A., Lee, C.-T.A., 2006. Geochemical investigation of serpentinized oceanic lithospheric mantle in the Feather River Ophiolite, California: implications for the recycling rate of water by subduction. Chem. Geol. 235, 161-185.

Lindsley, D.H., Dixon, S.A., 1976. Diopside-enstatite equilibria at 850 degrees to 1400 degrees C, 5 to 35 kb. Am. J. Sci. 276, 1285-1301.

Ling, M.-X., Sedaghatpour, F., Teng, F.-Z., Hays, P.D., Strauss, J., Sun, W., 2011.

Homogeneous magnesium isotopic composition of seawater: an excellent geostandard for Mg isotope analysis. Rapid Commun. Mass Spectrom. 25, 2828-2836.

Liu, C.-Z., Snow, J.E., Hellebrand, E., Brügmann, G., von der Handt, A., Büchl, A., Hofmann, A.W., 2008. Ancient, highly heterogeneous mantle beneath Gakkel ridge, Arctic Ocean. Nature 452, 311-316.

Liu, S.-A., Teng, F.-Z., He, Y., Ke, S., Li, S., 2010. Investigation of magnesium isotope fractionation during granite differentiation: implication for Mg isotopic composition of the continental crust. Earth Planet. Sci. Lett. 297, 646-654.

Liu, S.-A., Teng, F.-Z., Yang, W., Wu, F.-Y., 2011. High-temperature inter-mineral magnesium isotope fractionation in mantle xenoliths from the North China craton. Earth Planet. Sci. Lett. 308, 131-140.

Liu, X.-M., Teng, F.-Z., Rudnick, R.L., McDonough, W.F., Cummings, M.L., 2014. Massive magnesium depletion and isotope fractionation in weathered basalts. Geochim. Cosmochim. Acta 135, 336-349.

Malvoisin, B., 2015. Mass transfer in the oceanic lithosphere: Serpentinization is not isochemical. Earth Planet. Sci. Lett. 430, 75-85.

Mével, C., 2003. Serpentinization of abyssal peridotites at mid-ocean ridges. C. R. Geosci. 335, 825-852.

Meyzen, C.M., Ludden, J.N., Humler, E., Luais, B., Toplis, M.J., Mével, C., Storey, M., 2005. New insights into the origin and distribution of the DUPAL isotope anomaly in the Indian Ocean mantle from MORB of the Southwest Indian Ridge. Geochem. Geophy. Geosy. 6.

Michael, P., Langmuir, C., Dick, H., Snow, J., Goldstein, S., Graham, D., Lehnert, K., Kurras, G., Jokat, W., Mühe, R., 2003. Magmatic and amagmatic seafloor generation at the ultraslow-spreading Gakkel Ridge, Arctic Ocean. Nature 423, 956-961.

Moody, J.B., 1976. Serpentinization: a review. Lithos 9, 125-138.

Opfergelt, S., Georg, R., Delvaux, B., Cabidoche, Y.-M., Burton, K., Halliday, A., 2012. Mechanisms of magnesium isotope fractionation in volcanic soil weathering sequences, Guadeloupe. Earth Planet. Sci. Lett. 341, 176-185.

Paulick, H., Bach, W., Godard, M., De Hoog, J., Suhr, G., Harvey, J., 2006. Geochemistry of abyssal peridotites (Mid-Atlantic Ridge, 15 20′ N, ODP Leg 209): implications for fluid/rock interaction in slow spreading environments. Chem. Geol. 234, 179-210.

Prichard, H. M., 1979. A petrographic study of the process of serpentinisation in ophiolites and the ocean crust. Contrib. Mineral. Petrol. 68, 231-241.

Rudnick, R.L., McDonough, W.F., Chappell, B.W., 1993. Carbonatite metasomatism in the northern Tanzanian mantle: petrographic and geochemical characteristics. Earth Planet. Sci. Lett. 114, 463-475.

Schauble, E.A., 2011. First-principles estimates of equilibrium magnesium isotope fractionation in silicate, oxide, carbonate and hexaaquamagnesium (2+) crystals. Geochim. Cosmochim. Acta 75, 844-869.

Seyler, M., Cannat, M., Mevel, C., 2003. Evidence for major-element heterogeneity in

701 the mantle source of abyssal peridotites from the Southwest Indian Ridge (52^{o}
702 to 68^{o} E). Geochem. Geophy. Geosy. 4.
703 Shen, B., Jacobsen, B., Lee, C.-T.A., Yin, Q.-Z., Morton, D.M., 2009. The Mg
704 isotopic systematics of granitoids in continental arcs and implications for the role
705 of chemical weathering in crust formation. Proc. Natl. Acad. Sci. 106,
706 20652-20657.
707 Snow, J.E., Dick, H.J., 1995. Pervasive magnesium loss by marine weathering of
708 peridotite. Geochim. Cosmochim. Acta 59, 4219-4235.
709 Su, B.-X., Teng, F.-Z., Hu, Y., Shi, R.-D., Zhou, M.-F., Zhu, B., Liu, F., Gong, X.-H.,
710 Huang, Q.-S., Xiao, Y., 2015. Iron and magnesium isotope fractionation in
711 oceanic lithosphere and sub-arc mantle: Perspectives from ophiolites. Earth
712 Planet. Sci. Lett. 430, 523-532.
713 Teng, F.-Z., Hu, Y., Chauvel, C., 2016. Magnesium isotope geochemistry in arc
714 volcanism. Proc. Natl. Acad. Sci. 113, 7082-7087.
715 Thiede, J. et al., 2002. POLARSTERN ARKTIS XVII/2: Cruise Report: AMORE
716 2001 (Arctic Mid-Ocean Ridge Expedition). Berichte zur Polar-und
717 Meeresforschung (Reports on Polar and Marine Research) 421.
718 Teng, F.-Z., Li, W.-Y., Ke, S., Marty, B., Dauphas, N., Huang, S., Wu, F.-Y.,
719 Pourmand, A., 2010a. Magnesium isotopic composition of the Earth and
720 chondrites. Geochim. Cosmochim. Acta 74, 4150-4166.
721 Teng, F.-Z., Li, W.-Y., Rudnick, R.L., Gardner, L.R., 2010b. Contrasting lithium and
722 magnesium isotope fractionation during continental weathering. Earth Planet. Sci.
723 Lett. 300, 63-71.
724 Teng, F.-Z., Li, W.-Y., Ke, S., Yang, W., Liu, S.-A., Sedaghatpour, F., Wang, S.-J.,
725 Huang, K.-J., Hu, Y., Ling, M.-X., Xiao, Y., Liu, X.-M., Li, X.-W., Gu, H.-O.,
726 Sio, C.K., Wallace, D.A., Su, B.-X., Zhao, L., Chamberlin, J., Harrington, M.,
727 Brewer, A., 2015. Magnesium isotopic compositions of international geological
728 reference Materials. Geostand. Geoanal. Res. 39, 329-339.
729 Teng, F.-Z., Wadhwa, M., Helz, R.T., 2007. Investigation of magnesium isotope
730 fractionation during basalt differentiation: Implications for a chondritic
731 composition of the terrestrial mantle. Earth Planet. Sci. Lett. 261, 84-92.
732 Teng, F.-Z., Yang, W., 2014. Comparison of factors affecting the accuracy of
733 high-precision magnesium isotope analysis by multi-collector inductively
734 coupled plasma mass spectrometry. Rapid Commun. Mass Spectrom. 28, 19-24.
735 Teng, F.-Z., 2017. Magnesium isotope geochemistry, Rev. Mineral. Geochem. 82,
736 219-287.
737 Thompson, G., Melson, W.G., 1970. Boron contents of serpentinites and metabasalts
738 in the oceanic crust: implications for the boron cycle in the oceans. Earth Planet.
739 Sci. Lett. 8, 61-65.
740 Tipper, E., Galy, A., Gaillardet, J., Bickle, M., Elderfield, H., Carder, E., 2006. The
741 magnesium isotope budget of the modern ocean: constraints from riverine
742 magnesium isotope ratios. Earth Planet. Sci. Lett. 250, 241-253.
743 Wang, S.-J., Teng, F.-Z., Li, S.-G., 2014. Tracing carbonate–silicate interaction during
744 subduction using magnesium and oxygen isotopes. Nat. Commun. 5.

Wang, Z.-Z., Liu, S.-A., Ke, S., Liu, Y.-C., Li, S.-G., 2016. Magnesium isotopic heterogeneity across the cratonic lithosphere in eastern China and its origins. Earth Planet. Sci. Lett. 451, 77-88.

Warren, J.M., Shimizu, N., Sakaguchi, C., Dick, H.J., Nakamura, E., 2009. An assessment of upper mantle heterogeneity based on abyssal peridotite isotopic compositions. J. Geophys. Res.: Solid Earth (1978–2012) 114.

Wells, P.R., 1977. Pyroxene thermometry in simple and complex systems. Contrib. Mineral. Petrol. 62, 129-139.

Williams, H.M., Bizimis, M., 2014. Iron isotope tracing of mantle heterogeneity within the source regions of oceanic basalts. Earth Planet. Sci. Lett. 404, 396-407.

Wimpenny, J., Harvey, J., Yin, Q., 2012. The effects of serpentinization on Mg isotopes in Mid-Atlantic ridge peridotite, AGU Fall Meeting Abstracts, p. 1700.

Xiao, Y., Teng, F.-Z., Zhang, H.-F., Yang, W., 2013. Large magnesium isotope fractionation in peridotite xenoliths from eastern North China craton: product of melt-rock interaction. Geochim. Cosmochim. Acta 115, 241-261.

Yang, W., Teng, F.-Z., Zhang, H.-F., Li, S.-G., 2012. Magnesium isotopic systematics of continental basalts from the North China craton: Implications for tracing subducted carbonate in the mantle. Chem. Geol. 328, 185-194.

Yang, W., Teng, F.-Z., Zhang, H.-F., 2009. Chondritic magnesium isotopic composition of the terrestrial mantle: a case study of peridotite xenoliths from the North China craton. Earth Planet. Sci. Lett. 288, 475-482.

Yaxley, G.M., Crawford, A.J., Green, D.H., 1991. Evidence for carbonatite metasomatism in spinel peridotite xenoliths from western Victoria, Australia. Earth Planet. Sci. Lett. 107, 305-317.

Zhou, H.Y., Dick, H.J.B., 2013. Thin crust as evidence for depleted mantle supporting the MarionRise. Nature 494, 195-200.

Figure captions

Fig. 1 Physiographic and geoid maps of (a) the Gakkel Ridge in Arctic Ocean and (b) the SWIR in Indian and Atlantic Oceans with sample locations and petrographic pictures showing olivine (Ol), enstatite (Opx), diopside (Cpx) and spinel (Sp) in relatively fresh abyssal peridotites. Olivine sometimes can be altered along fractures.

Fig. 2 Back-scattered electron images showing various alteration minerals and

784 textures of the studied abyssal peridotites. (A) Primary minerals completely altered to
785 hornblende (Hbl), serpentine (Serp), chlorite (Chl) and andradite (And). (B) and (C)
786 Olivine (Ol) partially altered to serpentine and microcrystalline Fe-oxides and clay
787 (Fe-oxd+clay) aggregates. (D) Primary minerals altered to serpentine, hornblende and
788 chlorite.
789
790 Fig. 3 a-Bulk sample abyssal peridotite LOI values versus MgO contents showing a
791 negative correlation. b-Bulk sample abyssal peridotite δ^{26}Mg versus LOI values
792 showing a positive correlation for samples HLY and PS from Gakkel Ridge and 107
793 (represent AII107) from SWIR. Samples Pr from SWIR is largely within the Mg
794 isotopic range of mantle peridotites (δ^{26}Mg = -0.25±0.04‰) given by Teng et al.
795 (2010a) shown in the grey band.
796
797 Fig. 4 Plots of (a) SiO_2 versus CaO, (b) CaO versus Al_2O_3, (c) TiO_2 versus Al_2O_3 and
798 (d) TiO_2 versus δ^{26}Mg of abyssal peridotites recalculated to volatile free composition.
799 Symbols can be referred to Fig. 3.
800
801 Fig. 5 Comparison of measured (a) orthopyroxene (Opx) - olivine (Ol) fractionation
802 and (b) clinopyroxene (Cpx) - olivine (Ol) fractionation of Mg isotopes with
803 theoretical calculation as a function of temperature, and (c) plot of Cr# of spinel
804 versus whole-rock Mg isotopes for the studied relatively fresh abyssal peridotites. The
805 grey band represents Mg isotopic range of subcontinental mantle peridotites given by
806 Teng et al. (2010a). Uncertainties of Δ^{26}Mg values quote 2SD and are calculated as
807 the square root of the sum of the square of individual errors for δ^{26}Mg values.
808 Theoretical calculation of Mg isotopic fractionation is according to Schauble (2011).
809
810 Fig. 6 a-Plot of Al_2O_3/SiO_2 versus MgO/SiO_2 used to quantitatively measure the
811 departure of the peridotite MgO/SiO_2 ratio from the primary ratio of each sample
812 estimated from the MgO/SiO_2 versus Al_2O_3/SiO_2 terrestrial geochemical fractionation

array (Hart and Zindler, 1986; Jagoutz et al., 1979), assuming that Al and Si are immobile during marine weathering. b-Plot of $\delta^{26}Mg$ versus MgO/SiO_2* for abyssal peridotites. MgO/SiO_2*, the proxy for weathering, is a quantitative measure of the departure of the measured peridotite MgO/SiO_2 ratio from the primary ratio of each sample estimated from Fig. 6a. c-Plot of $\delta^{26}Mg$ versus MgO of abyssal peridotites showing a broadly negative correlation. Grey area represents mantle peridotite Mg isotopic compositions given by Teng et al. (2010a).

Fig. 7 Mg concentration normalized to primary Mg content (MgO = 44 wt.%) of fresh mantle peridotite reconstructed by Snow and Dick (1995) versus $\delta^{26}Mg$ for abyssal peridotites from Gakkel Ridge and SWIR. Curved lines illustrate Mg removal via Rayleigh distillation for different values of the fractionation factor α ($\alpha = (^{26}Mg/^{24}Mg)_{abyssal\ peridotite} / (^{26}Mg/^{24}Mg)_{fluid}$). Rayleigh distillation equation: $\delta^{26}Mg_{abyssal\ peridotite} = (\delta^{26}Mg_{mantle\ peridotite} +1000)f^{(1/\alpha-1)} -1000$; f - the fraction of Mg remaining in the rock, calculated from $MgO_{mantle\ peridotite}$ / 44 (primary MgO content of mantle peridotite); $\delta^{26}Mg_{mantle\ peridotite}$ = -0.25 ‰ (Teng et al., 2010a). Red square represents composition of average mantle peridotites. The abyssal peridotites in this study are plotted between α = 1.0002 to 1.001. Symbols can be referred to Fig. 3.

Tables

Table 1 Magnesium isotopic compositions of abyssal peridotites and standards

Table 2 Magnesium isotopic compositions of mineral separates and equilibrium temperatures for the studied abyssal peridotites

Appendix

Appendix 1 Major element compositions of abyssal peridotites

842

843 Appendix 2 EPM mineral compositions of olivine, enstatite, diopside and spinel in the

844 studied abyssal peridotites

Table 1

Table 1 Magnesium isotopic compositions of abyssal peridotites and standards

Sample/standard	^{26}Mg(‰)	2SD	^{25}Mg(‰)	2SD
Gakkel Ridge (84.83°N,4.66°E)				
HLY 4-37	-0.04	0.06	-0.04	0.04
HLY 4-37 rc	-0.05	0.06	-0.04	0.05
HLY 4-63	-0.14	0.07	-0.08	0.04
HLY 4-3	-0.01	0.07	0.01	0.04
HLY 4-29	-0.05	0.06	-0.01	0.04
Gakkel Ridge (85.44°N,14.52°E)				
HLY 40-26	-0.04	0.06	-0.02	0.05
HLY 40-53	-0.15	0.07	-0.08	0.04
HLY 40-56	-0.18	0.06	-0.08	0.04
HLY 40-43	-0.08	0.06	-0.04	0.04
Gakkel Ridge (84.64°N, 4.22°E)				
PS59 235-1	-0.14	0.06	-0.08	0.04
PS59 235-4	-0.14	0.07	-0.07	0.04
PS59 235-18	-0.13	0.06	-0.05	0.04
PS59 235-40	-0.10	0.07	-0.05	0.04
PS59 235-56	-0.09	0.06	-0.02	0.04
PS59 235-82	-0.08	0.06	-0.03	0.04
PS59 235-67	-0.12	0.06	-0.06	0.04
PS59 235-68	-0.07	0.06	-0.03	0.04
SWIR, Shaka FZ (53.38°S, 9.33°E)				
AII107 60-3	-0.07	0.06	-0.04	0.04
AII107 60-4	-0.15	0.07	-0.07	0.04
AII107 60-6	-0.09	0.07	-0.05	0.04
AII107 60-68	-0.16	0.06	-0.07	0.04
AII107 60-31	0.03	0.07	0.02	0.04
AII107 60-31 ra	-0.01	0.06	-0.01	0.05
AII107 60-31 rc	0.03	0.07	0.02	0.04
AII107 61-12	-0.03	0.07	-0.01	0.05
AII107 61-12 rc	-0.01	0.06	0.00	0.05
AII107 61-82	-0.14	0.06	-0.08	0.04
AII107 61-82 rc	-0.19	0.07	-0.11	0.04
AII107 61-98	-0.21	0.06	-0.11	0.04
AII107 61-98 ra	-0.20	0.05	-0.08	0.03
AII107 63-28	-0.08	0.06	-0.05	0.04
SWIR, Prince Edward FZ(46.54°S, 33.79°E)				
Pr 18-12	-0.14	0.07	-0.06	0.05
Pr 18-30	-0.18	0.07	-0.10	0.04
Pr 18-40	-0.21	0.07	-0.11	0.04
Pr 19-4	-0.18	0.07	-0.10	0.04
Pr 19-5	-0.16	0.07	-0.09	0.04
Pr 19-47	-0.22	0.07	-0.11	0.04
Pr 19-96	-0.24	0.07	-0.11	0.04
Pr 19-96 ra	-0.21	0.05	-0.09	0.03
Standards				
San Carlos olivine	-0.24	0.06	-0.12	0.04
n=6	-0.22	0.07	-0.13	0.05
	-0.23	0.07	-0.11	0.04
	-0.22	0.08	-0.10	0.07
	-0.21	0.07	-0.06	0.04
	-0.19	0.06	-0.09	0.05
Recommended	-0.24	0.03	-0.12	0.02
Hawaiian seawate	-0.84	0.09	-0.44	0.06
n=5	-0.81	0.07	-0.43	0.05
	-0.89	0.07	-0.44	0.04
	-0.79	0.08	-0.38	0.05
	-0.88	0.06	-0.47	0.05
Recommended	-0.83	0.09	-0.43	0.06
JB-1 basalt	-0.24	0.09	-0.12	0.06
Recommended	-0.276	###	-0.146	###

rc = repeat column chemistry from another aliquot of dissolved sample solution;

ra = repeat instrumental analysis on the same Mg-cut solution.

FZ = Fracture Zone

Recommended Mg isotopic compositions of San Carlos olivine, Hawaiian seawater and JB-1 basalt are from Hu et al. (2016b), Ling et al. (2011) and Teng et al. (2015), respectively.

Table 2

Table 2 Magnesium isotopic compositions of mineral separates and equilibrium temperatures for the studied abyssal peridotites

Sample	mineral	vol%[a]	δ^{26}Mg(‰)	2SD	δ^{25}Mg(‰)	2SD	Mg#	Cr#(Sp)	T (ºC)[b]	δ^{26}Mg(wr)[c]
Lherzolite										
PS59 235-1	Ol	84.4	-0.23	0.07	-0.09	0.04	90.8	0.14	1004	-0.22
	Opx	6.9	-0.17	0.07	-0.09	0.04	90.5			
	Cpx	8.6	-0.09	0.07	-0.05	0.04	91.0			
	Cpx ra	8.6	-0.06	0.05	-0.05	0.03				
PS59 235-4	Ol	59.0	-0.21	0.07	-0.11	0.04	89.7	0.3	1032	-0.22
	Opx	18.5	-0.27	0.07	-0.11	0.04	90.0			
	Cpx	22.5	-0.19	0.07	-0.12	0.04	89.9			
PS59 235-56	Ol	74.8	-0.18	0.07	-0.08	0.04	90.2	0.13	1065	-0.18
	Opx	20.7	-0.16	0.07	-0.10	0.04	90.1			
	Opx ra	20.7	-0.13	0.05	-0.09	0.03				
	Cpx	4.5	-0.16	0.07	-0.09	0.04	90.6			
PS59 235-82	Ol	56.5	-0.12	0.06	-0.05	0.05	91.1	0.21	1005	-0.13
	Ol ra	56.5	-0.10	0.05	-0.06	0.03				
	Opx	35.7	-0.17	0.06	-0.07	0.05	91.0			
	Cpx	7.8	-0.11	0.05	-0.06	0.03	92.1			
	Cpx ra	7.8	-0.12	0.06	-0.04	0.05				
HLY 4-63	Ol	70.3	-0.22	0.06	-0.12	0.05	89.7	0.38	1016	-0.22
	Opx	17.4	-0.17	0.06	-0.09	0.05	90.0			
	Cpx	12.3	-0.23	0.06	-0.12	0.05	90.7			
Cpx-bearing Harzburgite										
Pr 19-5	Ol	86.6	-0.30	0.06	-0.16	0.05	90.6	0.3	903	-0.29
	Opx	11.0	-0.20	0.06	-0.09	0.05	90.8			
	Cpx	2.4	-0.17	0.06	-0.09	0.05	91.8			
Harzburgite										
HLY 40-56	Ol	89.5	-0.19	0.06	-0.09	0.05	91.8	0.54	1041	-0.19
	Opx	10.5	-0.17	0.05	-0.08	0.03	92.1			

ra = repeat instrumental analysis on the same Mg-cut solution.

[a] Volume estimates of each sample is calculated by point counting of ~4×2.5 cm^2 thin section.

[b] T estimates of lherzolite and Cpx-bearing harzburgite are calculated according to Wells (1977), and those of harzburgite are according to Lindsley and Dixon (1976).

[c] wr-whole rock; δ^{26}Mg(wr) is calculated according to the volume, MgO content and Mg isotopic value of each constituting mineral.

Figure 1

Click here to download high resolution image

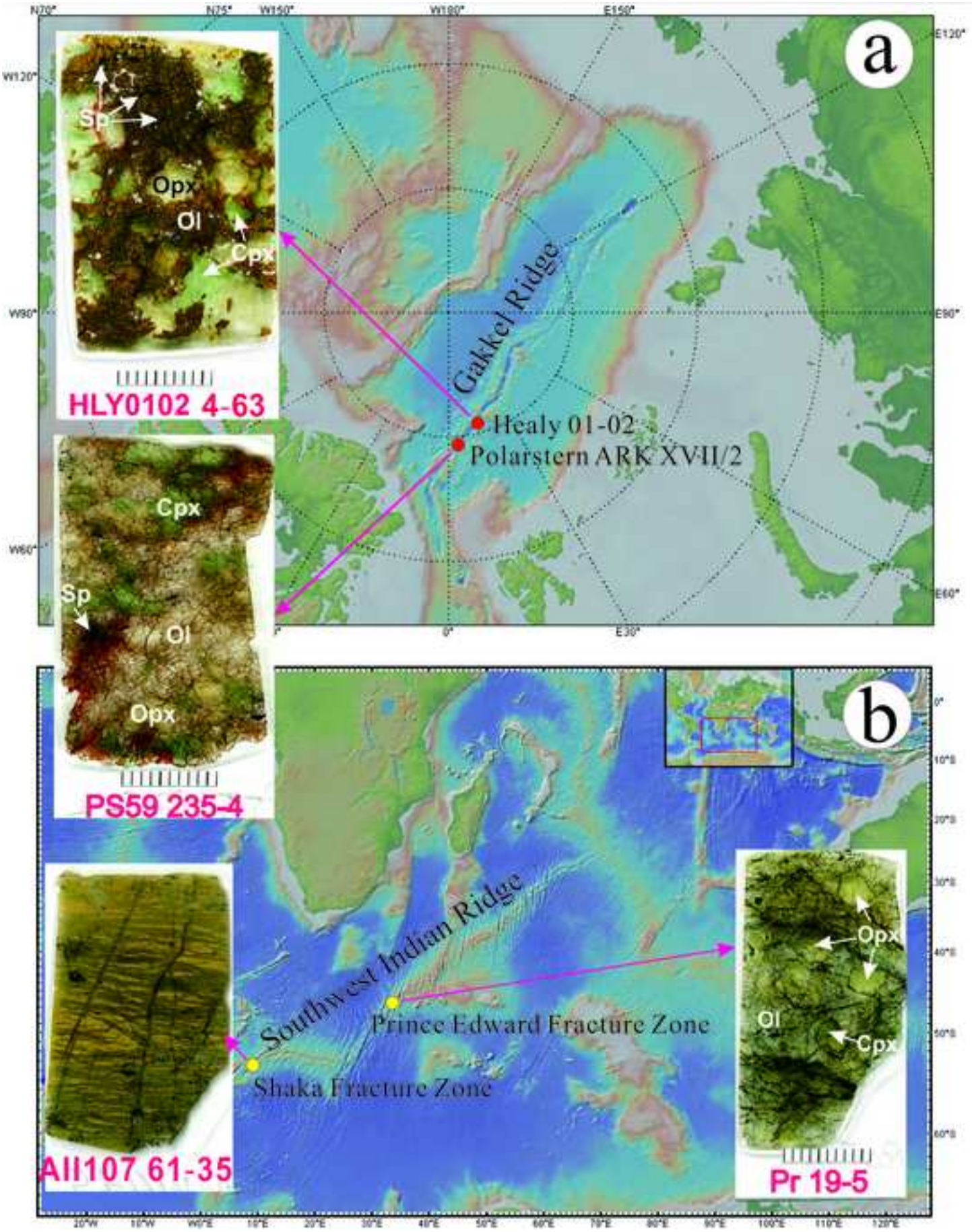

Figure 2

Click here to download high resolution image

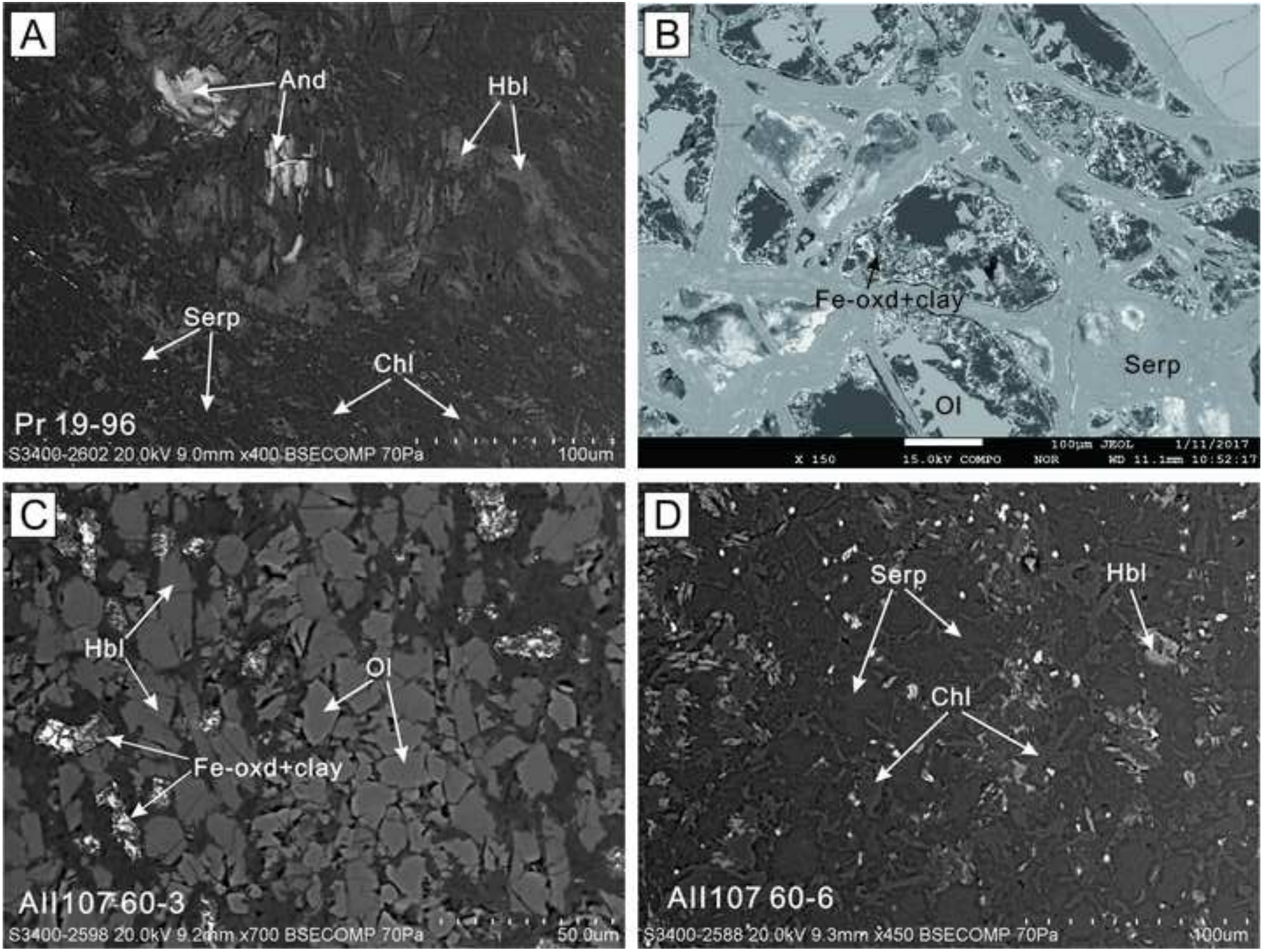

Figure 3

Click here to download high resolution image

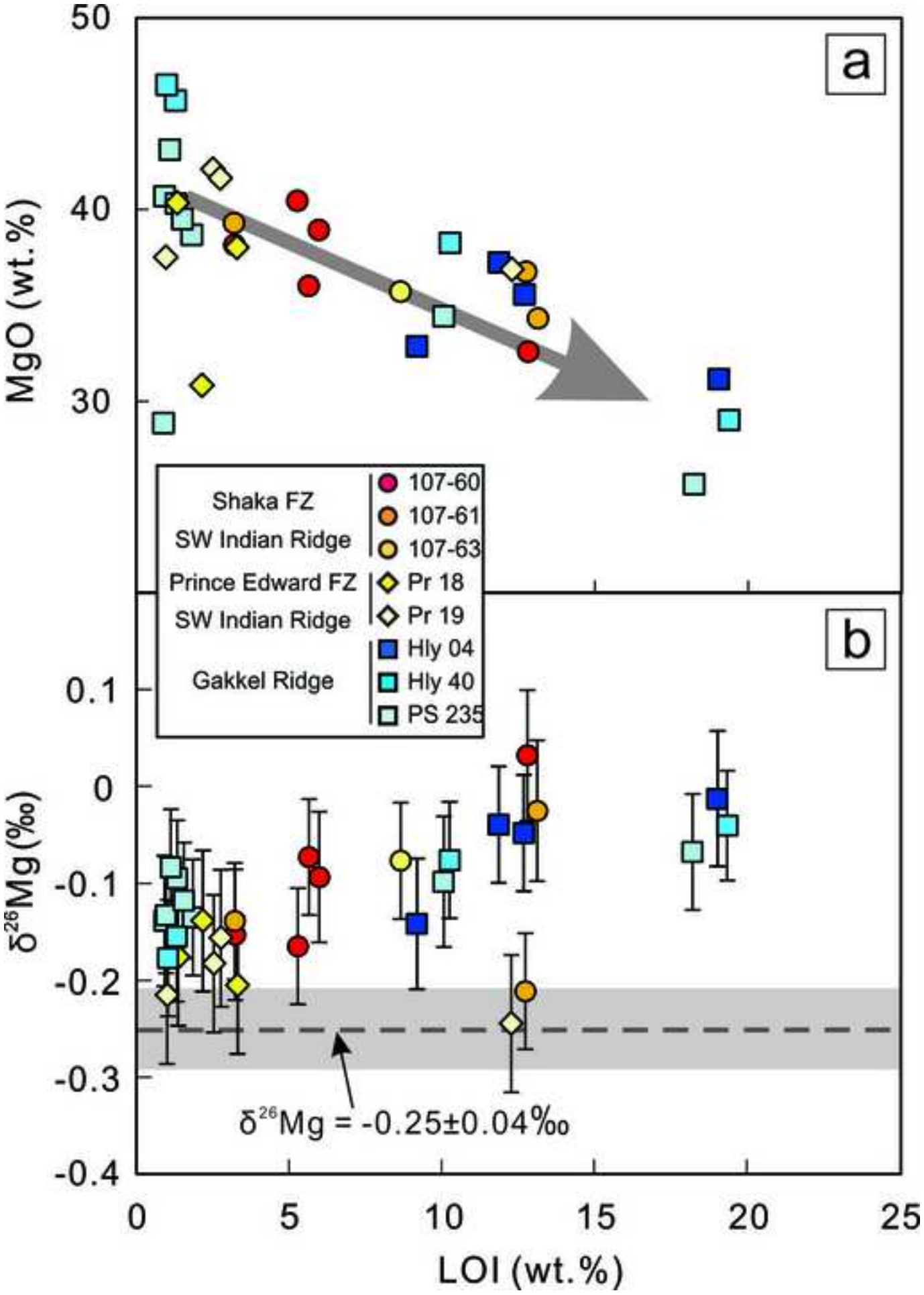

Figure 4

Click here to download high resolution image

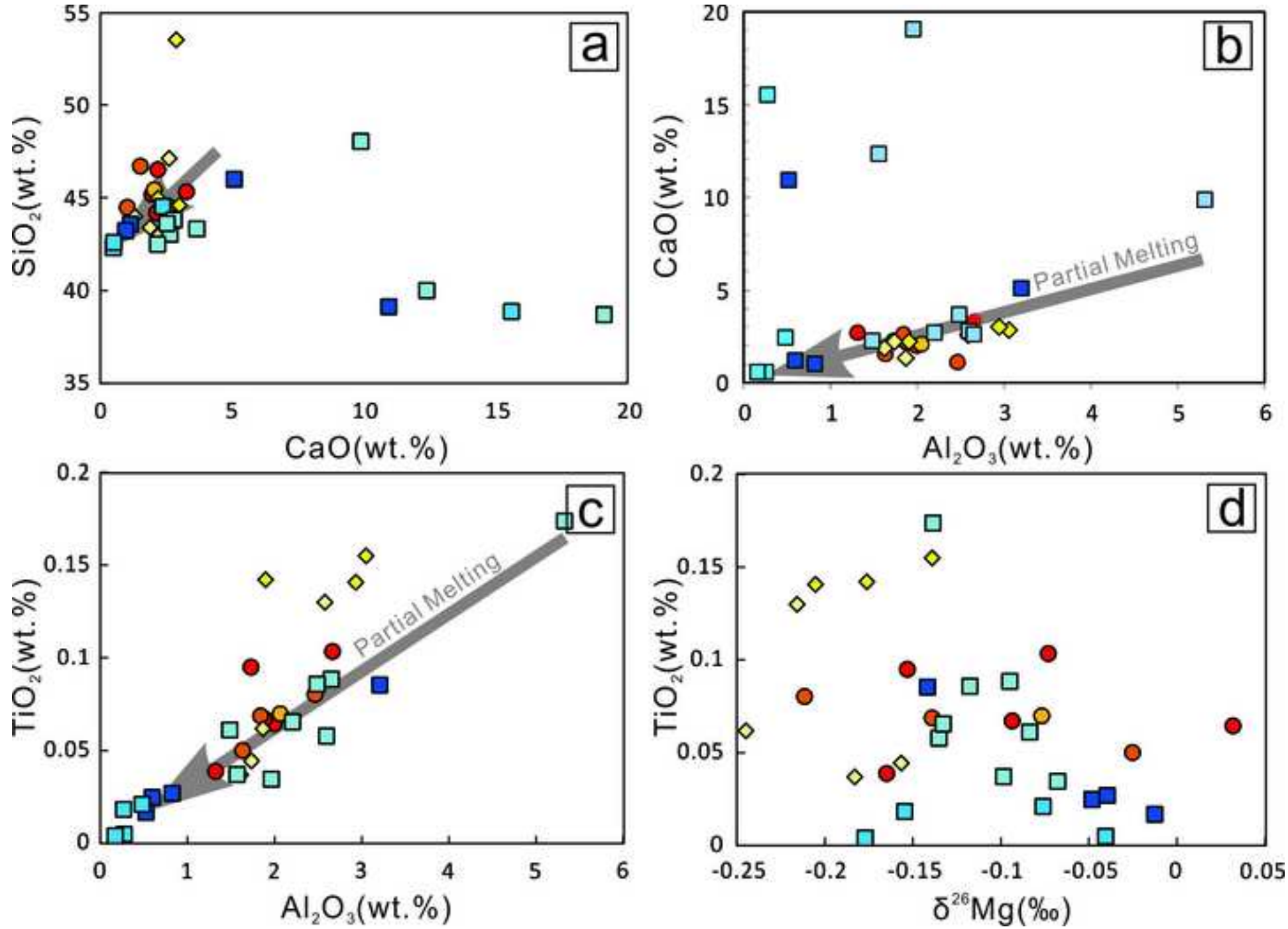

Figure 5

Click here to download high resolution image

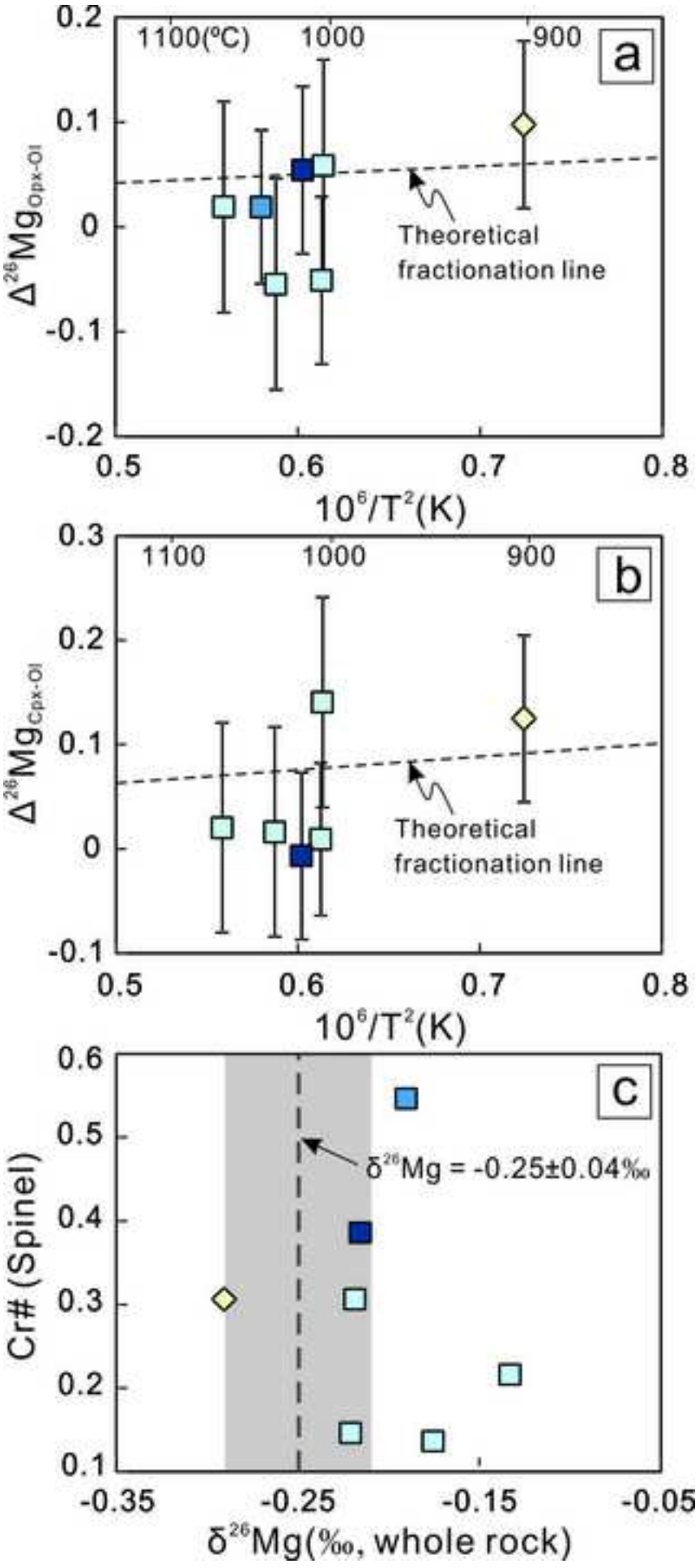

Figure 6

Click here to download high resolution image

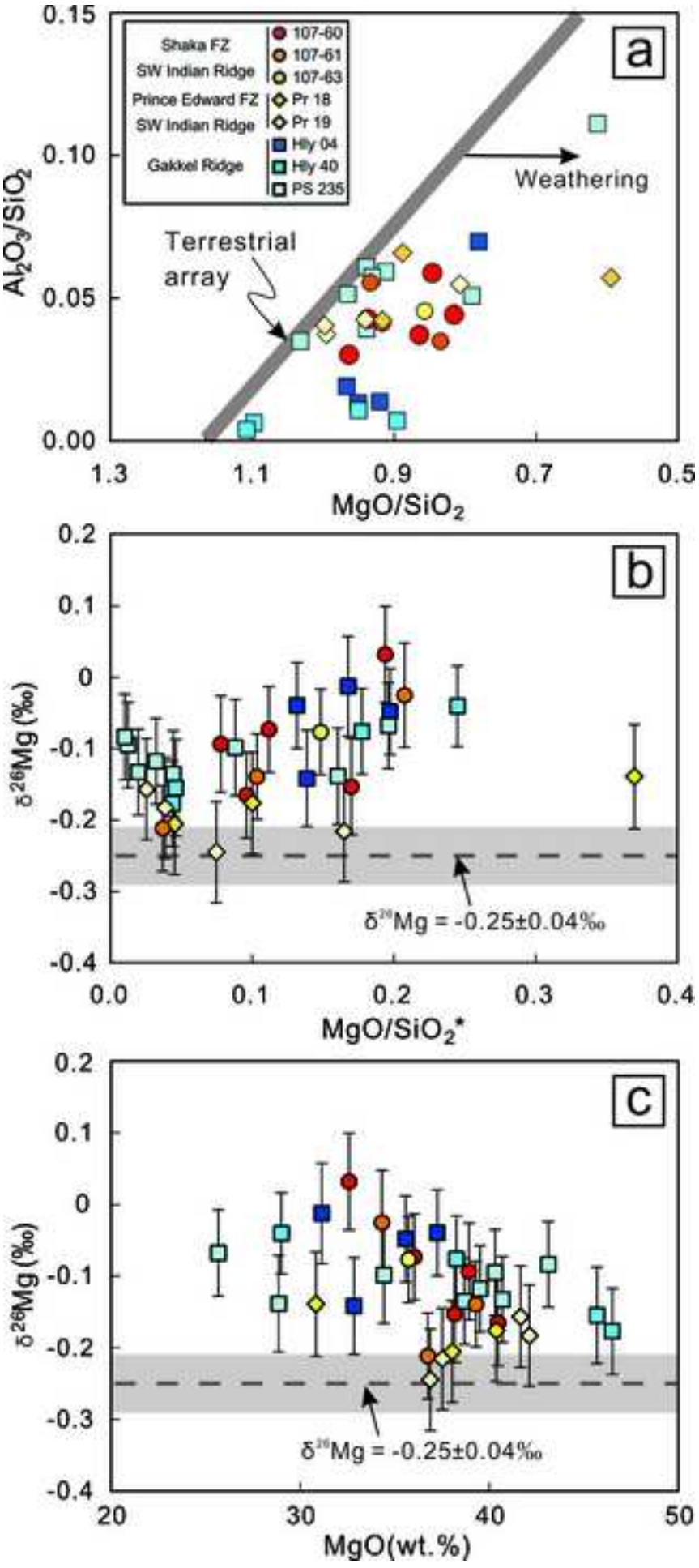

Figure 7

Click here to download high resolution image